Solid-State Structures

DOI: 10.1002/ange.201411008

A Robust Microfluidic Device for the Synthesis and Crystal Growth of Organometallic Polymers with Highly Organized Structures**

Xiao Liu, Qiaolian Yi, Yongzhen Han, Zhenning Liang, Chaohua Shen, Zhengyang Zhou, Junliang Sun, Yizhi Li, Wenbin Du, and Rui Cao**

Abstract: *A simple and robust microfluidic device was developed to synthesize organometallic polymers with highly organized structures. The device is compatible with organic solvents. Reactants are loaded into pairs of reservoirs connected by a 15 cm long microchannel prefilled with solvents, thus allowing long-term counter diffusion for self-assembly of organometallic polymers. The process can be monitored, and the resulting crystalline polymers are harvested without damage. The device was used to synthesize three insoluble silver acetylides as single crystals of X-ray diffraction quality. Importantly, for the first time, the single-crystal structure of silver phenylacetylide was determined. The reported approach may have wide applications, such as crystallization of membrane proteins, synthesis and crystal growth of organic, inorganic, and polymeric coordination compounds, whose single crystals cannot be obtained using traditional methods.*

Since its discovery a century ago[1] X-ray crystallography has been one of the major driving forces for continuous evolution of chemistry, structural biology, and materials science. A major bottleneck for structure determination is obtaining high-quality single crystals which can diffract to atomic resolution, and it remains a costly and time-consuming process which often generates unpredictable outcomes. In the last decade, microfluidics has quickly emerged as an outstanding platform to boost the efficiency and rate of success in growing crystals.[2,3] A variety of microfluidic devices, using flow-,[4] droplet-,[5–8] valve-,[9,10] diffusion-,[11] or well-based[12–15] approaches, have been developed to screen crystallization conditions in small volumes, and have been successful in growing crystals of proteins,[9] nanoparticles,[16–18] and metal–organic frameworks.[19,20] However, the use of microfluidics still falls short on several key aspects. First, versatility of microfluidic platforms is seriously restricted by their limited tolerance and stability against organic solvents, especially for devices fabricated with polydimethylsiloxanes and plastics.[3] Second, growth of single crystals of complexes with poor solubility is extremely difficult using flow- or droplet-based methods because of instant precipitation. Examples include many compounds with polymeric structures and many kinds of inorganic and organometallic salts. Third, self-assembly of coordination polymers with highly organized structures is a research area of great interest and significance, but devices for the synthesis of polymeric complexes as single crystals suitable for X-ray diffraction have not yet been established. Hitherto, there is still an unmet need for developing robust platforms which have good solvent compatibility for growing single crystals of inorganic, organic, and metal–organic materials with high regularity. Such platforms should also allow convenient harvesting of the target crystals for X-ray diffraction.

Organometallics are extensively used in stoichiometric and catalytic processes and materials science. Silver acetylides are among the oldest organometallics known[21] and have attracted immense attention because of their unique catalytic features,[21–23] as well as various binding modes and intrinsic structural properties.[24–27] As the key intermediates in alkyne activation, silver acetylides are very mild and have very low basicity, and thus are very useful in the synthesis of complex molecules.[28–34] However, because of their low solubility and explosive and reactive nature, the structural information on these intermediates is rare, but critical to better understand their catalysis. In contrast, silver acetylides, especially silver phenylacetylide (SPA), are fundamental building blocks for the construction of diverse silver chains, high-nuclearity silver clusters and cages,[25,35–39] and have been used to prepare silver nanowires.[40] Considerable efforts have been made to elucidate the structural aspects of SPA. In 2005, Che and coworkers proposed a polymeric chain structure based on X-ray powder diffraction data and a model derived from its copper congener.[41] However, despite the seminal work by the group

[*] X. Liu,[+] Prof. Dr. R. Cao
School of Chemistry and Chemical Engineering
Shaanxi Normal University, Xi'an 710062 (China)
E-mail: ruicao@ruc.edu.cn
X. Liu,[+] Y. Z. Han, Z. N. Liang, C. H. Shen, Prof. Dr. R. Cao
Department of Chemistry
Renmin University of China, Beijing 100872 (China)
Q. Yi,[+] Prof. Dr. W. Du
State Key Laboratory of Microbial Resources
Institute of Microbiology, Chinese Academy of Sciences
Beijing 100101 (China)
E-mail: wenbin@im.ac.cn
Z. Y. Zhou, Prof. Dr. J. L. Sun
College of Chemistry and Molecular Engineering
Peking University, Beijing 100871 (China)
Prof. Dr. Y. Z. Li
State Key Laboratory of Coordination Chemistry
Coordination Chemistry Institute
Nanjing University, Nanjing 210093 (China)
[+] These authors contributed equally to this work.

[**] We gratefully thank Prof. Yapei Wang for helpful discussions. This work is supported by grants from the "Thousand Young Talents" program in China, the National Natural Science Foundation of China (No. 21101170, 21205134 and 31230003), and the State Key Laboratory of Microbial Resources, Institute of Microbiology, Chinese Academy of Sciences (Grant SKLMR-20120604).
Supporting information for this article is available on the WWW under http://dx.doi.org/10.1002/anie.201411008.

of Che, a more accurate structure determination of SPA is still needed, and is highly challenging because SPA is explosive and insoluble, and precipitates immediately upon formation.

In this work, we report a glass-based microfluidic device which can tolerate a wide range of organic solvents. We introduce a bonding method based on an epoxy–amine linkage[42] to make the device accessible for direct crystal collection. Precise control of the counter-diffusion process[11,43] in microfluidics, a process which is achieved by a dynamic equilibrium between mass transport and aggregation kinetics, prevents precipitation and allows crystal growth of insoluble complexes. By using this device, we successfully synthesized three silver acetylides, including SPA, and elucidated their highly organized structures by single-crystal X-ray diffraction.

A glass microfluidic device was developed to synthesize insoluble organometallics as single crystals based on counter diffusion[43] (Figure 1), a contemporary crystallization technology which is considered to be able to minimize supersaturation and impurity levels at the crystal-growth front. The device is composed of two 75 mm × 25 mm × 1.8 mm glass plates bonded through epoxy–amine linkages. The top plate contains 15 cm long channels (400 μm in width, 150 μm in depth). Drilled holes (5.65 μL in volume) at each end of the channel are used as reservoirs to load samples. The bottom plate contains etched Arabic numbers (1 μm in depth) for addressing the locations of crystal growth. These markers are visible under microscope and are considered to have negligible effect on the crystallization process because of their very small depth compared to that of channels.

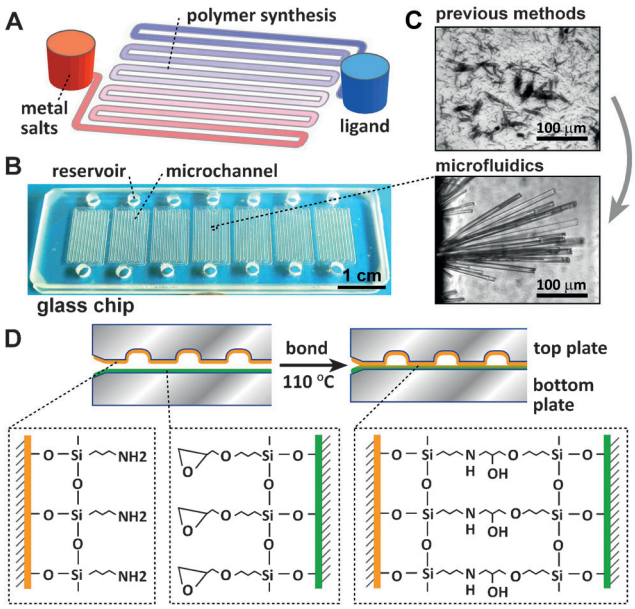

Figure 1. A) Device designed for the synthesis of organometallic polymers. B) Photograph of the device with seven parallel units with a zoomed-in view of the crystals of **1** within the channel. C) Photography of SPA quickly precipitated (top) and large single crystals of **1** formed in our device (bottom). D) Mechanism for reversible bonding of top and bottom glass plates with outstanding tolerance to organic solvents.

The device operation is simple and straightforward (see Figure S1 in the Supporting Information). To avoid rapid reaction and precipitation, channels were prefilled with the solvent to be used for synthesis. Solutions of metal salts (i.e., silver nitrate) and ligands (i.e., various acetylenes) were loaded into two reservoirs in sequence. To avoid solvent flow in the channel and ensure volume accuracy, before loading solution to one reservoir, we used a glass lid to cover the other reservoir. The lids were secured with paper clips after both reservoirs were loaded. A thin layer of fluorinated oil was then added to the gap between the device and lids to prevent evaporation of solvents. On a single device, we can set up seven individual experiments in parallel. All experiments were performed in the dark to avoid light-induced photoreduction of the silver acetylide crystals.

To make the device accessible, we introduced a novel method to reversibly bond glass plates. This accessible feature is critical for microfluidics to trace crystal growth and to select and pick up single crystals of X-ray diffraction quality. In a typical experiment, the top and bottom plates were silanized with monolayers of 3-aminopropyltrimethoxysilane (APTES) and 3-glycidoxypropyltrimethoxysilane (GPTS), respectively. The bonding was then realized at 110 °C through epoxy–amine linkages (Figure 1 D). The silanization and bonding processes were validated by surface studies of the glass plates using X-ray photoelectron spectroscopy (XPS; see the Supporting Information for details). As shown in Figures S2 and S3, silanization of glass-plate surfaces with APTES and GPTS resulted in a signal increase for N 1s (Figure S2B) and C 1s (for the C2/C3 atoms connected to oxygen atoms; Figure S3C), respectively, as compared to signals of the pristine glass plates (Figures S2A and Figure S3A, respectively). We bonded two glass plates with the APTES modification and GPTS modification together, ruptured the bonding between the two plates by opening the device with a razor blade, and analyzed the two glass-plate surfaces again. Significantly, XPS analysis of the surfaces of both glass plates after bonding and rupturing showed that the C 1s and N 1s XPS profiles of the two plates were almost identical to each other, and were different to the original profiles of the silanized glass plates. This result suggests the formation of epoxy–amine bonds between the two plates, and that the rupture of these bonds left homogeneous residues on both plates. This method for low-temperature reversible bonding of glass may be widely adopted for incorporating functional structures such as electronics,[44] waveguides,[45] biosensors,[46] and nanoassemblies[20] in glass-based microfluidic devices, and enabling in situ detection with instruments including MALDI mass spectrometry, atomic force microscopy, electrochemical scanning microscopy, etc.

To test the tolerance of this glass microfluidic device to organic solvents, we fabricated glass plates of 12 mm × 23 mm with monolayers of APTES and GPTS and with holes (0.8 mm of diameter) on the middle of one side, offset the position of two glass plates, and bonded them together with a contact area of about 2 cm^2 (see Figure S4A). The bonded devices were immersed in either deionized water or a variety of organic solvents, including acetonitrile, dichloromethane, methanol, dimethylformamide, and diethyl ether for 5 days at

room temperature. The maximum shear force for rupturing the bonds between the two plates was measured using a digital force gauge (Figure S4) as described.[47] Our bonding strength measurements showed that similar levels of shear forces ($>40\,N\,cm^{-2}$) were required to break the bonded glass devices immersed in different organic solvents and water (see Table S1). This result suggested that the glass microfluidic device exhibited excellent solvent tolerance, which is required in crystallization of inorganic, organic, and organometallic complexes.

This glass microfluidic device greatly increases the diffusion distance and reaction time by adopting the counter-diffusion configuration, in which reactants are injected to the opposite ends of the microchannel. Previous microfluidic devices usually have mixing or diffusion distances of tens to hundreds of micrometers, and it takes milliseconds to hours to reach the equilibration.[4–10,48,49] The counter-diffusion configuration supports longer mixing or diffusion distances on the centimeter scale and beyond. Previously, plastic chips or glass capillaries with counter-diffusion configurations have been developed. However, these devices are either incompatible with organic solvents or do not allow simple crystal collection. These issues are fully addressed in the current device.

To precisely control the diffusion equilibration to ensure slow self-assembly of polymeric organometallics, metal salts, and ligands were introduced to two reservoirs at the ends of the 15 cm long channel. Importantly, the channel was preloaded with organic solvents which allow the reaction of two compounds only after long-term counter diffusion. Based on Fick's law of diffusion, the diffusion time for a solute to pass through the microchannel is estimated as $t = x^2/(2D)$. Here, t is elapsed time, x is the diffusion distance, and D is the diffusion coefficient. For the synthesis of SPA, the theoretical diffusion coefficients[50] of $AgNO_3$ and phenylacetylene are known to be $5.6\times10^{-5}\,cm^2s^{-1}$ and $2.7\times10^{-5}\,cm^2s^{-1}$, respectively, and the estimated time for them to diffuse to the middle of channel (7.5 cm) is 5.8 and 12 days, respectively. It takes up to 48 days for phenylacetylene to diffuse across the 15 cm long channel. The concentration profiles of $AgNO_3$ and phenylacetylene diffusing through the channel prefilled with acetonitrile were numerically simulated (see Figure S5). At 24 hours, the intersection point of $AgNO_3$ and phenylacetylene was located at 8.9 cm from the access hole of $AgNO_3$ with about a 0.29% percentage. Single crystals were first observed after 4 days at the location close to the estimated intersection point where two components initially encountered to form SPA (Figure 2B). Our design greatly extends the equilibration and reaction time and enables slow self-assembly of highly organized polymeric structures, which cannot be obtained using traditional methods.

On-chip synthesis and crystallization of SPA were conducted. Prescreening of the loading concentrations of silver salts and acetylene ligands was first carried out to identify the appropriate conditions for synthesis and crystal growth (see Figure S6). It is worth noting that as silver acetylides are sensitive to light-induced photoreduction, all experiments were performed in the dark with care. Under optimized reaction conditions, needle-like crystals of $[Ag_8(PhC{\equiv}C)_8]_n$ (**1**) were observed in the channel with large crystals mainly

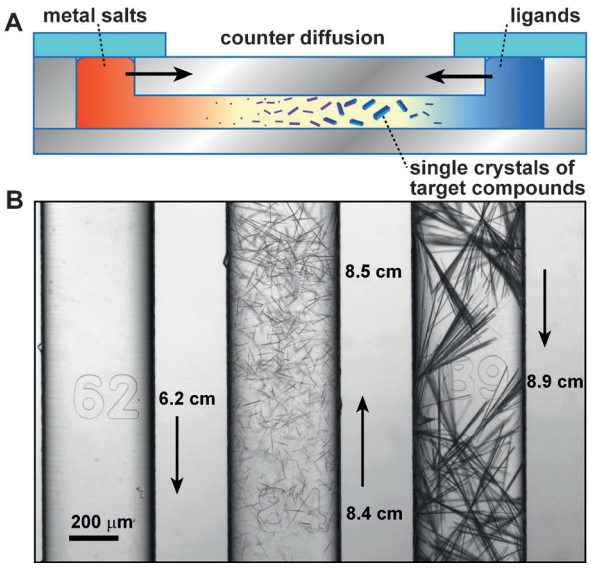

Figure 2. A) Counter diffusion and silver acetylide synthesis in the microchannel. B) Microphotograph shows the distribution and morphology of silver acetylide polymers along the microchannel.

located at the initial place of crystal growth (Figure 2). After opening the device using a razor blade, a crystal with a diameter of 17 μm and a length of 280 μm (Figure 1C) was selected for X-ray diffraction studies. The complex **1** crystallized in the monoclinic space group $P2_1/c$ (Table S2).[51] In the asymmetric unit there is an Ag_8 cluster assembled with eight $[PhC{\equiv}C]^-$ ligands (see Figure S7). The Ag_8 cluster can be viewed as two parallel Ag_4 rectangles which have about a 90° rotation from each other and stack along the *b* direction (Figure 3). One Ag_4 rectangle contains two μ_2-η^1,η^2 and two μ_3-η^1,η^1,η^1 $[PhC{\equiv}C]^-$ units, while the other contains four μ_3-η^1,η^1,η^1 $[PhC{\equiv}C]^-$ units. Two Ag_4 rectangles are connected through the bridging $[PhC{\equiv}C]^-$ ligands and Ag–Ag interactions, and the extension of Ag_8 along the *b* axis gives a highly organized silver cluster column.

Comparison of the single-crystal X-ray structure of **1** and previously proposed structure of SPA, based on X-ray powder diffraction studies by Che and co-workers,[41] revealed that they are different. In the structure of **1**, the repeat unit is a Ag_8 cluster assembled by two staggered Ag_4 rectangles with very short Ag–Ag distances of 2.896 and 2.868 Å. Whereas for the powder structure, the repeat unit is a diamond-like Ag_4 cluster with an average Ag–Ag distance of 3.11 Å. These results indicate that, stronger Ag–Ag interactions and tighter packing of polymeric silver chains are present in **1**.

As we expected, the calculated powder diffraction pattern of **1** does not match that experimentally observed by Che (see Figure S8). This result confirms that **1** is different to the previous powder sample of SPA. We rationalized that the synthesis and crystallization conditions to generate **1** and the powder sample of SPA are different. For example, the powder sample formed and precipitated in a few seconds from the reaction of $AgNO_3$ and phenylacetylene, while crystals of **1** were obtained by controlled reaction of these two reactants in more than 15 days. The slow reaction and longer crystal

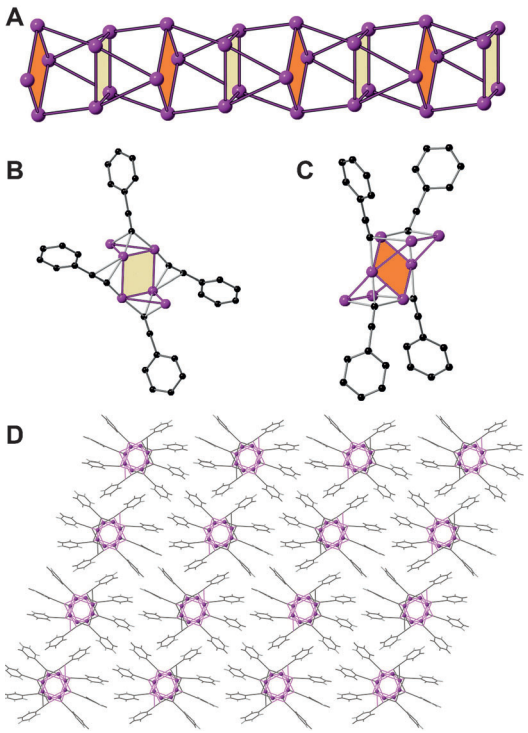

Figure 3. A) Silver chain structure of **1** showing two types of Ag_4 rectangles. B, C) The two Ag_4 rectangles. D) Packing diagram viewed along the *b* axis.

growth may permit tighter packing in **1**. To test this hypothesis, we mixed the reactants by liquid diffusion in a long-thin glass column. Thin crystalline needles were harvested within 5 days. Although they were not suitable for single-crystal X-ray diffraction, X-ray powder diffraction measurements showed that the sample was different compared to that of both **1** and the previous powder sample, thus indicating that the reaction and crystallization time play a key role in the construction of the polymeric structure of SPA.

In addition to **1**, synthesis and crystal growth of two new silver acetylides were achieved using this device. Reaction of naphthalene-based 1-$C_{10}H_7$-C≡CH and HC≡C-1,8-$C_{10}H_6$-C≡CH with $Ag(CF_3COO)$ gave $[Ag_{18}(1\text{-}C_{10}H_7\text{-}C{\equiv}C)_{12}(CF_3COO)_6]_n$ (**2**) and $[Ag_{11}\{(C{\equiv}C)\text{-}(1,8\text{-}C_{10}H_6)\text{-}(C{\equiv}C)\}_2(CF_3COO)_7]_n$ (**3**), respectively. The complex **2** crystallizes in the hexagonal space group $P6_3/m$ with organized silver chains along the *c* axis. The repeat unit consisted of $[Ag_{18}(1\text{-}C_{10}H_7\text{-}C{\equiv}C)_{12}(CF_3COO)_6]$ (see Figure S9). The ligand $[1\text{-}C_{10}H_7\text{-}C{\equiv}C]^-$ has only one μ_4-$\eta^1,\eta^1,\eta^1,\eta^2$ coordination mode. The silver chain of **2** can be viewed as a stack of two types of equilateral triangles (Figure 4). The Ag–Ag distances in these two triangles are 2.900 and 3.999 Å, and it is 3.018 Å between the two types of triangles. Figure 4C depicts the packing of the silver chains. Strong intermolecular C–H···π (2.424 Å) and π···π (2.608 Å) interactions are observed, thus revealing extensive interactions between naphthalene rings. The complex **3** crystallizes in the triclinic space group $P\bar{1}$ and has a silver chain structure along the *a* axis with a $[Ag_{11}\{(C{\equiv}C)\text{-}(1,8\text{-}C_{10}H_6)\text{-}(C{\equiv}C)\}_2(CF_3COO)_7]$ repeat unit (see Figure S10). The Ag_{11} aggregate connects to each other through Ag–Ag

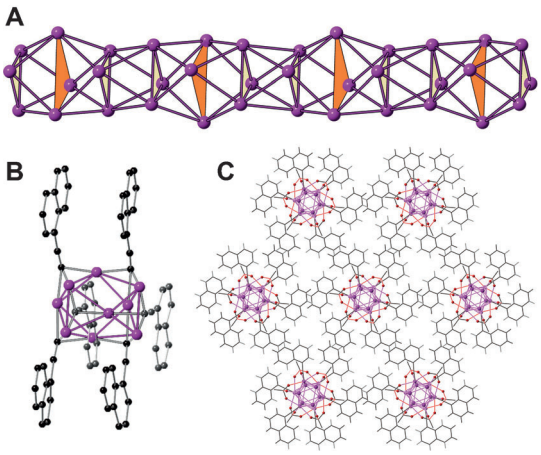

Figure 4. A) The silver chain structure of **2** showing two types of Ag_3 equilateral triangles. B) The Ag_9 cluster. C) Packing diagram viewed along *c* axis.

interactions and a bridging $[(C{\equiv}C)\text{-}(1,8\text{-}C_{10}H_6)\text{-}(C{\equiv}C)]^{2-}$ ligand. It is worth noting that silver naphthylacetylides are insoluble and sensitive to light-induced photoreduction, which make their crystal growth extremely challenging.

In conclusion, the success of making **1**–**3** shows that this newly developed glass microfluidic device is useful for growing crystals which were previously difficult to obtain. The compatibility with organic solvents, the convenience for crystal harvest, the well-controlled reaction and crystal growth, and the simplicity of fabrication and usage make this device valuable for synthesis and crystallization of insoluble and reactive complexes, and complexes and materials (e.g., coordination polymers, reaction intermediates, organometallics, membrane proteins, and supramolecular complexes) which are not soluble in aqueous solutions. The structure of **1** is the first single-crystal X-ray structure of SPA, and will substantially contribute to our understanding of its catalytic properties and the process to form other silver clusters and cages. Differences between **1** and the powder sample, precipitated from direct mixing, imply that a slow reaction and crystallization process give a more condensed silver column structure. The highly organized polymeric structures reported in this work are extremely challenging, if at all possible, to generate using traditional methods, and further highlights the significance of this device for self-assembly of polymeric structures. As silver nanowires trace the shape of the starting materials (i.e., silver acetylide crystals),[40] this feature may shed light on the development of simplified assembly of various silver nanowire materials.

Received: November 13, 2014
Published online: December 12, 2014

Keywords: crystal growth · polymers · silver · solid-state structures · X-ray diffraction

[1] S. W. Wilkins, *Acta Crystallogr. Sect. A* **2013**, *69*, 1–4.
[2] J. Leng, J. B. Salmon, *Lab Chip* **2009**, *9*, 24–34.

[3] J. Puigmartí-Luis, *Chem. Soc. Rev.* **2014**, *43*, 2253 – 2271.
[4] T. L. Sounart, P. A. Safier, J. A. Voigt, J. Hoyt, D. R. Tallant, C. M. Matzke, T. A. Michalske, *Lab Chip* **2007**, *7*, 908 – 915.
[5] B. Zheng, J. D. Tice, L. S. Roach, R. F. Ismagilov, *Angew. Chem. Int. Ed.* **2004**, *43*, 2508 – 2511; *Angew. Chem.* **2004**, *116*, 2562 – 2565.
[6] L. Li, D. Mustafi, Q. Fu, V. Tereshko, D. L. Chen, J. D. Tice, R. F. Ismagilov, *Proc. Natl. Acad. Sci. USA* **2006**, *103*, 19243 – 19248.
[7] D. Witters, S. Vermeir, R. Puers, B. F. Sels, D. E. De Vos, J. Lammertyn, R. Ameloot, *Chem. Mater.* **2013**, *25*, 1021 – 1023.
[8] D. Witters, N. Vergauwe, R. Ameloot, S. Vermeir, D. De Vos, R. Puers, B. Sels, J. Lammertyn, *Adv. Mater.* **2012**, *24*, 1316 – 1320.
[9] C. L. Hansen, E. Skordalakes, J. M. Berger, S. R. Quake, *Proc. Natl. Acad. Sci. USA* **2002**, *99*, 16531 – 16536.
[10] C. L. Hansen, S. Classen, J. M. Berger, S. R. Quake, *J. Am. Chem. Soc.* **2006**, *128*, 3142 – 3143.
[11] J. D. Ng, P. J. Clark, R. C. Stevens, P. Kuhn, *Acta Crystallogr. Sect. D* **2008**, *64*, 189 – 197.
[12] X. C. Zhou, L. Lau, W. W. L. Lam, S. W. N. Au, B. Zheng, *Anal. Chem.* **2007**, *79*, 4924 – 4930.
[13] W. B. Du, L. Li, K. P. Nichols, R. F. Ismagilov, *Lab Chip* **2009**, *9*, 2286 – 2292.
[14] L. Li, W. B. Du, R. F. Ismagilov, *J. Am. Chem. Soc.* **2010**, *132*, 106 – 111.
[15] L. Li, W. B. Du, R. F. Ismagilov, *J. Am. Chem. Soc.* **2010**, *132*, 112 – 119.
[16] M. I. Bodnarchuk, L. Li, A. Fok, S. Nachtergaele, R. F. Ismagilov, D. V. Talapin, *J. Am. Chem. Soc.* **2011**, *133*, 8956 – 8960.
[17] J. Angly, A. Iazzolino, J. B. Salmon, J. Leng, S. P. Chandran, V. Ponsinet, A. Désert, A. Le Beulze, S. Mornet, M. Tréguer-Delapierre, M. A. Correa-Duarte, *ACS Nano* **2013**, *7*, 6465 – 6477.
[18] J. Puigmartí-Luis, M. Rubio-Martínez, I. Imaz, B. Z. Cvetković, L. Abad, A. P. del Pino, D. Maspoch, D. B. Amabilino, *ACS Nano* **2014**, *8*, 818 – 826.
[19] M. Faustini, J. Kim, G. Y. Jeong, J. Y. Kim, H. R. Moon, W. S. Ahn, D. P. Kim, *J. Am. Chem. Soc.* **2013**, *135*, 14619 – 14626.
[20] J. Puigmartí-Luis, M. Rubio-Martínez, U. Hartfelder, I. Imaz, D. Maspoch, P. S. Dittrich, *J. Am. Chem. Soc.* **2011**, *133*, 4216 – 4219.
[21] U. Halbes-Letinois, J. M. Weibel, P. Pale, *Chem. Soc. Rev.* **2007**, *36*, 759 – 769.
[22] Y. Yamamoto, *Chem. Rev.* **2008**, *108*, 3199 – 3222.
[23] J. M. Weibel, A. Blanc, P. Pale, *Chem. Rev.* **2008**, *108*, 3149 – 3173.
[24] L. Zhao, T. C. W. Mak, *J. Am. Chem. Soc.* **2005**, *127*, 14966 – 14967.
[25] L. Zhao, X. L. Zhao, T. C. W. Mak, *Chem. Eur. J.* **2007**, *13*, 5927 – 5936.
[26] C. Y. Gao, L. Zhao, M. X. Wang, *J. Am. Chem. Soc.* **2012**, *134*, 824 – 827.
[27] C. Y. Gao, L. Zhao, M. X. Wang, *J. Am. Chem. Soc.* **2011**, *133*, 8448 – 8451.
[28] D. Tejedor, S. López-Tosco, F. Cruz-Acosta, G. Méndez-Abt, F. García-Tellado, *Angew. Chem. Int. Ed.* **2009**, *48*, 2090 – 2098; *Angew. Chem.* **2009**, *121*, 2124 – 2131.
[29] P. de Armas, D. Tejedor, F. García-Tellado, *Angew. Chem. Int. Ed.* **2010**, *49*, 1013 – 1016; *Angew. Chem.* **2010**, *122*, 1029 – 1032.
[30] C. He, S. Guo, J. Ke, J. Hao, H. Xu, H. Y. Chen, A. W. Lei, *J. Am. Chem. Soc.* **2012**, *134*, 5766 – 5769.
[31] J. Q. Liu, Z. X. Fang, Q. Zhang, Q. Liu, X. H. Bi, *Angew. Chem. Int. Ed.* **2013**, *52*, 6953 – 6957; *Angew. Chem.* **2013**, *125*, 7091 – 7095.
[32] M. Gao, C. He, H. Y. Chen, R. P. Bai, B. Cheng, A. W. Lei, *Angew. Chem. Int. Ed.* **2013**, *52*, 6958 – 6961; *Angew. Chem.* **2013**, *125*, 7096 – 7099.
[33] M. B. Zhou, R. J. Song, C. Y. Wang, J. H. Li, *Angew. Chem. Int. Ed.* **2013**, *52*, 10805 – 10808; *Angew. Chem.* **2013**, *125*, 11005 – 11008.
[34] Y. Unoh, K. Hirano, T. Satoh, M. Miura, *Angew. Chem. Int. Ed.* **2013**, *52*, 12975 – 12979; *Angew. Chem.* **2013**, *125*, 13213 – 13217.
[35] J. Qiao, K. Shi, Q. M. Wang, *Angew. Chem. Int. Ed.* **2010**, *49*, 1765 – 1767; *Angew. Chem.* **2010**, *122*, 1809 – 1811.
[36] S. D. Bian, H. B. Wu, Q. M. Wang, *Angew. Chem. Int. Ed.* **2009**, *48*, 5363 – 5365; *Angew. Chem.* **2009**, *121*, 5467 – 5469.
[37] P. S. Cheng, S. Marivel, S. Q. Zang, G. G. Gao, T. C. W. Mak, *Cryst. Growth Des.* **2012**, *12*, 4519 – 4529.
[38] S. D. Bian, J. H. Jia, Q. M. Wang, *J. Am. Chem. Soc.* **2009**, *131*, 3422 – 3423.
[39] B. Li, R. W. Huang, H. C. Yao, S. Q. Zang, T. C. W. Mak, *CrystEngComm* **2014**, *16*, 723 – 729.
[40] J. Nishijo, O. Oishi, K. Judai, N. Nishi, *Chem. Mater.* **2007**, *19*, 4627 – 4629.
[41] S. S. Y. Chui, M. F. Y. Ng, C. M. Che, *Chem. Eur. J.* **2005**, *11*, 1739 – 1749.
[42] L. Tang, N. Y. Lee, *Lab Chip* **2010**, *10*, 1274 – 1280.
[43] F. Otálora, J. A. Gavira, J. D. Ng, J. M. García-Ruiz, *Prog. Biophys. Mol. Biol.* **2009**, *101*, 26 – 37.
[44] M. Q. Xue, Z. Xie, L. S. Zhang, X. L. Ma, X. L. Wu, Y. G. Guo, W. G. Song, Z. B. Li, T. B. Cao, *Nanoscale* **2011**, *3*, 2703 – 2708.
[45] P. Fei, Z. T. Chen, Y. F. Men, A. Li, Y. R. Shen, Y. Y. Huang, *Lab Chip* **2012**, *12*, 3700 – 3706.
[46] Y. Shen, Y. Y. Liu, G. Zhu, H. Fang, Y. H. Huang, X. Y. Jiang, Z. L. Wang, *Nanoscale* **2013**, *5*, 527 – 531.
[47] Z. J. Jia, Q. Fang, Z. L. Fang, *Anal. Chem.* **2004**, *76*, 5597 – 5602.
[48] X. Mu, W. F. Zheng, L. Xiao, W. Zhang, X. Y. Jiang, *Lab Chip* **2013**, *13*, 1612 – 1618.
[49] C. H. Shen, P. Xu, Z. Huang, D. Y. Cai, S. J. Liu, W. B. Du, *Lab Chip* **2014**, *14*, 3074 – 3080.
[50] F. Amemiya, H. Matsumoto, K. Fuse, T. Kashiwagi, C. Kuroda, T. Fuchigami, M. Atobe, *Org. Biomol. Chem.* **2011**, *9*, 4256 – 4265.
[51] Crystal data for **1**: $[C_{64}H_{40}Ag_8]$, monoclinic, $P2_1/c$, $a = 26.204(2)$, $b = 5.8803(15)$, $c = 36.090(2)$ Å, $\beta = 109.813(3)$, $V = 5231.9(14)$ Å^3, $Z = 4$, $T = 153(2)$ K, 19332 reflections collected, 10293 unique ($R_{int} = 0.0146$), final $R1 = 0.0542$, $wR2 = 0.1426$ for 6882 observed reflections [$I > 2\sigma(I)$]. Crystal data for **2**, $[C_{78}H_{46}Ag_9F_9O_8]$, hexagonal, $P6_3/m$, $a = 17.6170(7)$, $c = 13.7406(9)$ Å, $V = 3693.2(3)$ Å^3, $Z = 2$, $T = 150(2)$ K, 73081 reflections collected, 2666 unique ($R_{int} = 0.0572$), final $R1 = 0.0531$, $wR2 = 0.1385$ for 1766 observed reflections [$I > 2\sigma(I)$]. Crystal data for **3**, $[C_{55}H_{42}Ag_{11}Cl_2F_{21}N_4O_{19}]$, triclinic, $P\bar{1}$, $a = 8.2079(3)$, $b = 15.6831(6)$, $c = 28.3950(11)$ Å, $\alpha = 85.488(2)$, $\beta = 85.2450(10)$, $\gamma = 86.8800(10)$, $V = 3627.1(2)$ Å^3, $Z = 2$, $T = 150(2)$ K, 102429 reflections collected, 14838 unique ($R_{int} = 0.0412$), final $R1 = 0.0369$, $wR2 = 0.0830$ for 12371 observed reflections [$I > 2\sigma(I)$]. CCDC 1020984 (**1**), 1020985 (**2**) and 1020986 (**3**) contains the supplementary crystallographic data for this paper. These data can be obtained free of charge from The Cambridge Crystallographic Data Centre via www.ccdc.cam.ac.uk/data_request/cif.